Development of a Consequent Pole Transverse Flux Permanent Magnet Linear Machine with Passive Secondary Structure

Jun Luo, Baoquan Kou, He Zhang, and Ronghai Qu
(Invited)

***Abstract*—Transverse-flux machines have the advantage of high force density owing to the peculiarity of decoupling of electric loading and magnetic loading. In this paper, a novel consequent-pole transverse-flux permanent magnet linear machine (CP-TFPMLM) is proposed and investigated. The origination of the proposed machine is from an existing transverse-flux flux-reversal linear machine (TF-FRLM), by partially replacing permanent magnet poles with soft magnetic iron for further reducing the cost of magnets. The fundamental structure and operating principle are introduced at first. The electromagnetic performance, including back EMF, detent force, and thrust force, are investigated with the finite element method. The proposed machine can achieve similar performance as compared to the TF-FRLM but with half of the magnets are used.**

***Index Terms*—Consequent pole, linear machine, primary PM, transverse flux.**

I. INTRODUCTION

TRANSVERSE flux machines (TFM), with main magnetic flux path flowing perpendicular to the direction of motion, have the advantage of decoupled electric loading and magnetic loading, which makes it possible to further improve the force density by decreasing the pole pitch and increasing the pole number [1]-[4]. Compared with the conventional machines, transverse flux machines are more prominent in high force density, design flexibility, and cost-effective advantages [5]-[7]. Therefore, they are extensively researched all over the world.

Linear transverse flux machine integrates the direct-drive merit of linear machine and the high force density merit of the transverse-flux machine, hence, it is well suitable for low speed linear drive applications. Scholars have taken a large effort to improve and optimize the topologies of the transverse flux permanent magnet linear machines (TFPMLM) for different purposes. Kou *et al* proposed a bidirectional cross-linking TFPMLM to ensure all the magnetic flux under coupling surface interlink with the winding, which will improve the machine's inner space utilization and obtain a high force density [8]. Shin *et al* [9] proposed a double-sided TFPMLM to address the complex structure of transverse flux machinery, and the method for cogging force reduction was investigated in [10], and the design method for high force-to-weight ratio and low material cost was analyzed in [11]. For simplifying the manufacturing process, Zou *et al* [12] proposed a tubular TFPMLM, of which the primary core is made by laminated steel as same to the conventional rotary machines. The mature processing technology of traditional machines can be used in making transverse flux machines. The approach to suppress inter-pole flux linkage was investigated in [13] by introducing iron bridges, however, the overall structure of the machine became complex. The aforementioned TFPMLMs have permanent magnets and winding on separate side of the machine. By moving the magnets to the same side with armature coils, the secondary side can be further simplified, that is crucial for linear machines of long stator configuration. For long stroke applications, this kind machines can save manufacturing costs. Kang *et al* have investigated a TFPMLM with short primary for railway traction [14, 15]. The air gap flux density is improved by the gathering magnetic flux effect, hence higher force density can be achieved. But the structure of the twisted secondary cores seems to be a little complex and is hard for manufacturing. By applying the flux reversal theory in conventional machines into the transverse flux machine, a transverse-flux flux-reversal linear machine was proposed in [16]. Without twisting either the primary core or the secondary core, the TF-FRLM has a more simplified structure and is easy for fabricating. Furthermore, a flux switching TFPMLM was proposed in [17] combining the high force density advantage of transverse flux linear machine and the simple structure advantage of flux-switching linear machine.

Recent research papers [18]-[19] reveal that the consequent pole structure can achieve less permanent magnet material usage [20]-[21] and improve the field weakening capability and power density [22] by few impacting of the other electromagnetic performances. Up to now, the applications of consequent-pole structure are mainly focused on the synchronous motors, namely, the magnets and windings are separately placed on stator or mover. And the transverse-flux

Manuscript was submitted for review on 30, January, 2019.
This work was supported by the National Natural Science Foundation of China under Grant 51520105010.
Jun Luo, Baoquan Kou, and He Zhang are with the Department of Electrical Engineering, Harbin Institute of Technology, Harbin 150001, China (e-mail: luojunlj@163.com; koubq@hit.edu.cn; antonyamanda@163.com).
Ronghai Qu is with the School of Electrical and Electronic Engineering, Huazhong University of Science and Technology, Wuhan 430074, China (e-mail: ronghaiqu@hust.edu.cn).
Digital Object Identifier 10.30941/CESTEMS.2019.00006

motors with consequent-pole structure have barely been widely investigated as the traditional longitudinal-flux motors.

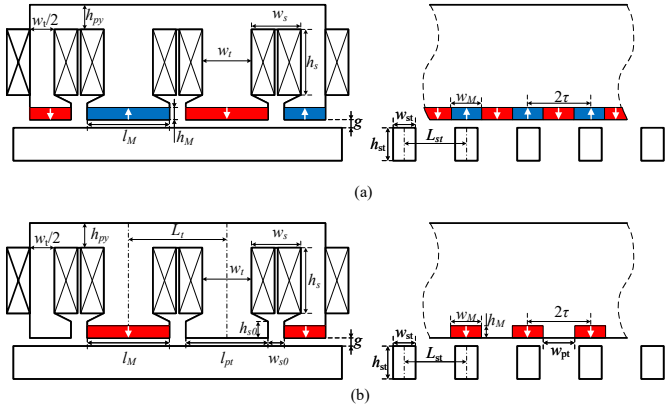

Fig. 1. Transverse-flux linear motor with different permanent magnet arrangement topologies. (a) Conventional TF-FRLM. (b) Consequent pole TFPMLM.

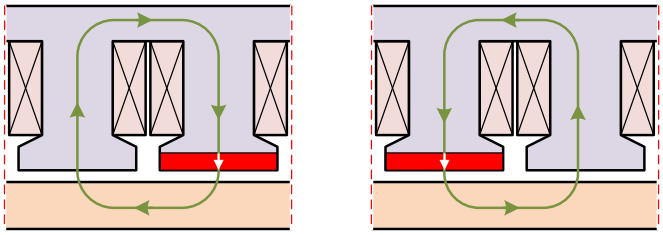

Fig. 2 The magnetic path in the CP TFPMLM. (a) The positive maximum flux linkage. (b) The negative maximum flux linkage.

In this paper, a consequent-pole transverse flux permanent magnet linear machine is proposed and investigated. Firstly, the basic structure and operating principle are introduced. Then, the equivalent magnetic circuit is established. The flux linkage, back EMF, as well as thrust force expressions are deduced. Thirdly, the electromagnetic performance is investigated based on a three-dimensional FEM model, and the comparisons are made. Finally, some conclusions are drawn based on the analysis.

II. Configuration and Operating Principle

Fig. 1 presents the cross-section view of the proposed structure and its counterpart. The consequent-pole TFPMLM is originated from the topology of the TF-FRLM by substituting half of the primary magnets with magnetic cores as shown in Fig. 1 (b). All the left magnets have the same direction of magnetization. The formative shallow teeth are sandwiched by magnets, and are magnetized with the opposite polarity compared to the magnets. The basic operation principle of the proposed machine is similar to the TF-FRLM as shown in Fig. 2. According to the principle of minimum reluctance, the flux produced by permanent magnets prefers accomplishing its path with the maximum permeance. As different magnets on nearby primary teeth are in alignment with secondary core, the flux-linkage in the coil will reverse its direction.

When the winding is motivated, the armature reaction field distribution is established. As the ferrimagnetic pole is high permeable, most of the armature flux goes through the iron pole as depicted in Fig. 3 in the CP TFPMLM. The existence of ferrimagnetic poles reduces the total reluctance faced by the armature reaction field. Hence, the armature reaction field

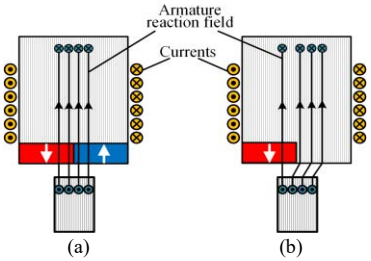

Fig. 3. Armature reaction fields in different types of TFLMs. (a) Conventional TF-FRLM. (b) Consequent pole TPMLM.

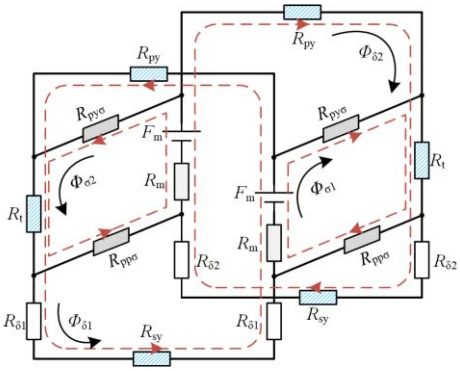

Fig. 4. Equivalent magnetic circuit of the CP TPMLM.

seems to be strengthened both in air gap and magnets areas. That's to say, the PMs are more likely to be demagnetized in the CP TFPMLM.

III. Equivalent Magnetic Circuit and Theoretical Analysis

Fig. 4 shows the equivalent magnetic circuit model of the proposed CP TFPMLM. Wherein, R_t, R_{py} represent the reluctance of primary tooth and primary yoke, respectively. R_m is the permanent magnet reluctance. R_δ is the air gap reluctance. R_{sy} is the secondary core reluctance. $R_{py\sigma}$ and $R_{pp\sigma}$ represent the leakage reluctance in the primary core and air gap, respectively.

The loop equations can be obtained by applying the Kirchhoff's law in magnetic circuit, there are

$$\begin{cases} (2R_{\delta 1}+R_{sy}+R_{py}+R_t+R_m)\Phi_{\delta 1}+R_m\Phi_{\sigma 1}+R_t\Phi_{\sigma 2}=F_m \\ (2R_{\delta 2}+R_{sy}+R_{py}+R_t+R_m)\Phi_{\delta 2}+R_t\Phi_{\sigma 1}+R_m\Phi_{\sigma 2}=F_m \\ R_m\Phi_{\delta 1}+R_t\Phi_{\delta 2}+(R_m+R_{py\sigma}+R_t+R_{pp\sigma})\Phi_{\sigma 1}=F_m \\ R_t\Phi_{\delta 1}+R_m\Phi_{\delta 2}+(R_m+R_{py\sigma}+R_t+R_{pp\sigma})\Phi_{\sigma 2}=F_m \end{cases} \quad (1)$$

where F_m is the equivalent magnetomotive force of the permanent magnet, and there is

$$F_m = H_c h_m \quad (2)$$

where H_c is the intrinsic coercivity of magnets, h_m is the height of the magnets in the direction of magnetization.

At no-load condition, the saturation in the magnetic core can be ignored, hence, the relevant reluctances with high permeance can be removed from (1), which gives

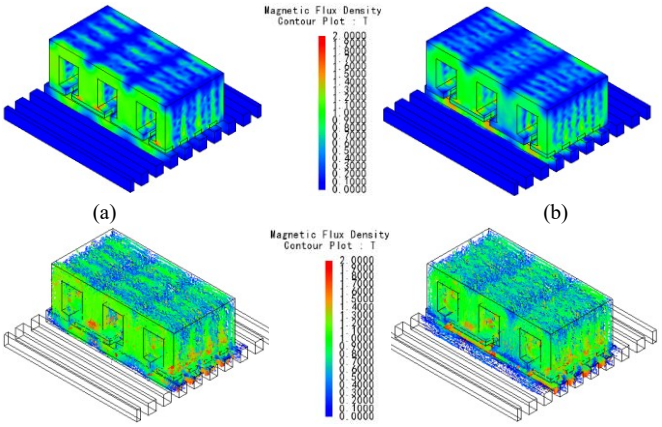

Fig. 5. Field distribution of the CP TPMLM at no-load condition. (a) Clouds map of flux density at x = 0. (b) Clouds map of flux density at x = τ/2. (c) Vector plot of flux density at x = 0. (d) Vector plot of flux density at x = τ/2.

$$\begin{cases} (2R_{\delta 1}+R_m)\Phi_{\delta 1}+R_m\Phi_{\sigma 1}=F_m \\ (2R_{\delta 2}+R_m)\Phi_{\delta 2}+R_m\Phi_{\sigma 2}=F_m \\ R_m\Phi_{\delta 1}+(R_m+R_{pp\sigma})\Phi_{\sigma 1}=F_m \\ R_m\Phi_{\delta 2}+(R_m+R_{pp\sigma})\Phi_{\sigma 2}=F_m \end{cases} \tag{3}$$

By solving (3), the main flux intertwining with the coil can be expressed as

$$\begin{cases} \Phi_{\delta 1}=\dfrac{F_m}{2R_{\delta 1}+R_m(1+2R_{\delta 1}/R_{pp\sigma})} \\ \Phi_{\delta 2}=\dfrac{F_m}{2R_{\delta 2}+R_m(1+2R_{\delta 2}/R_{pp\sigma})} \end{cases} \tag{4}$$

On account of the flux excited by different magnets flowing in opposite direction, the net flux linkage can be deduced as

$$\Phi_\delta=\Phi_{\delta 1}-\Phi_{\delta 2} = \frac{2F_m(R_{\delta 1}-R_{\delta 2})}{[2R_{\delta 1}+R_m(1+2R_{\delta 1}/R_{pp\sigma})][2R_{\delta 2}+R_m(1+2R_{\delta 1}/R_{pp\sigma})]} \tag{5}$$

Equation (5) shows that the total flux linkage produced by the magnets is mainly proportional to the difference of the air gap reluctance faced by each magnet. Along with the motion of the mover, the air gap reluctance varies with a period of 2τ (τ is the pole pitch), therefore, by neglecting the higher harmonic orders, the flux linkage can be expressed simply as

$$\Psi_c=N\Phi_m\cos\left(\frac{\pi}{\tau}x\right) \tag{6}$$

where N is the turns of each coil, and x is the displacement of the mover.

TABLE I.
PARAMETERS OF TRANSVERSE FLUX LINEAR MACHINE.

Symbol	Items	CP TFPMLM	TF-FRLM
p	Number of poles	4	
q	Number of primary teeth	4	
τ	Pole pitch (mm)	7.5	
w_s	Width of slot (mm)	20	
h_s	Height of slot (mm)	25	
l_M	Length of slot (mm)	34	
h_M	Height of slot (mm)	3	
g	Length of air gap (mm)	1	
w_{st}	Width of secondary core (mm)	7.5	
J	Current density (A/mm^2)	4.8	
N	Number of coils	120	

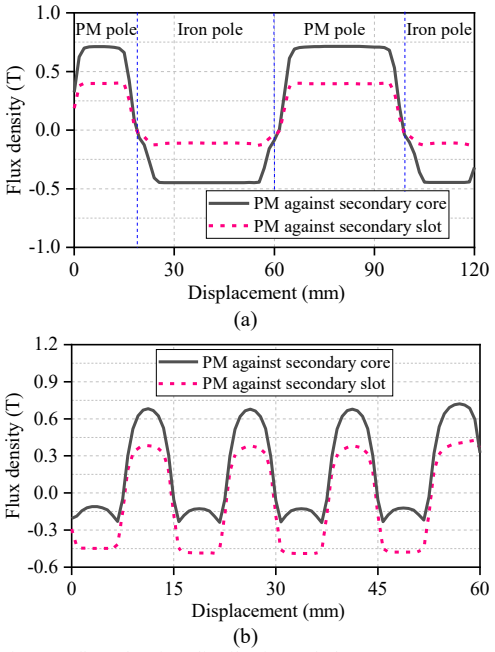

Fig. 6. Air gap flux density distribution of the CP TPMLM at no-load condition. (a) Displacement along transversal direction. (b) Displacement along longitudinal direction.

With the motion of the mover, the electromotive force will produce at the open-circuit coil ends according to Faraday's law, which gives

$$E=\frac{d\Psi_c}{dt}=\frac{\pi}{\tau}vN\Phi_m\sin\left(\frac{\pi}{\tau}x\right) \tag{7}$$

where v indicates the velocity of the mover.

When only the q-axis current is motivated, the thrust force will produce. For a three-phase CP TFPMLM, the thrust force can be deduced as

$$F=\frac{3\sqrt{2}\,\pi vNI\Phi_m}{2\tau} \tag{8}$$

where I is the root mean square value of applied current.

IV. PERFORMANCE EVALUATION

The field distribution of the TFPMLM is inherently three dimensional. Hence, it is hard to use 2-D finite element method (FEM) to investigated this kind machine, hence, the 3-D FEM is employed in this paper to fully consider the stray magnetic flux and leakage flux distribution. The fundamental parameters are listed in Table. I. In order to investigated the performance of the proposed consequent-pole machine, the same parameters are applied to a TF-FRLM.

A. Field Distribution

Fig. 5 depicts the no-load field distribution of the CP TFPMLM. The net magnetic flux linkage in the winding reaches the maximum value in Fig. 5(a) and (c), while it is zero in Fig. 5(b) and (d). The flux density in the primary tooth is about 1.2T. The highest flux density is about 1.6T on the corner of the tooth tip.

The normal component of air gap flux density are depicted in Fig. 6 both along transversal and longitudinal direction. As can

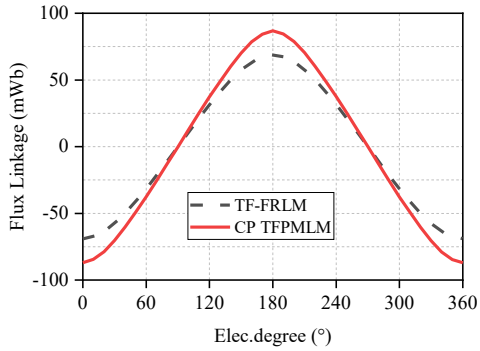

Fig. 7. Distribution of flux linkage waveforms.

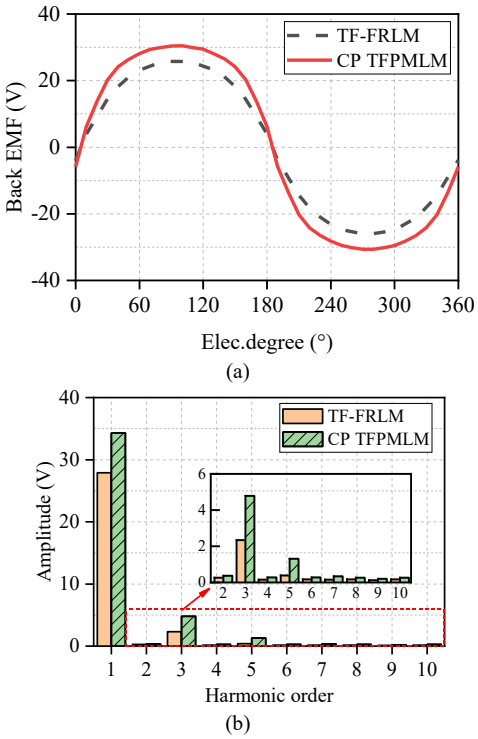

Fig. 8. Distribution of back EMF. (a) Waveforms distribution. (b) Harmonic order and amplitude distribution.

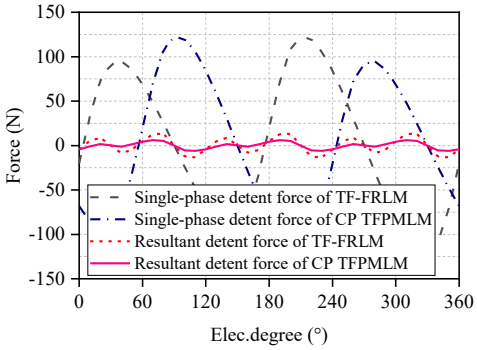

Fig. 9. Distribution of detent force.

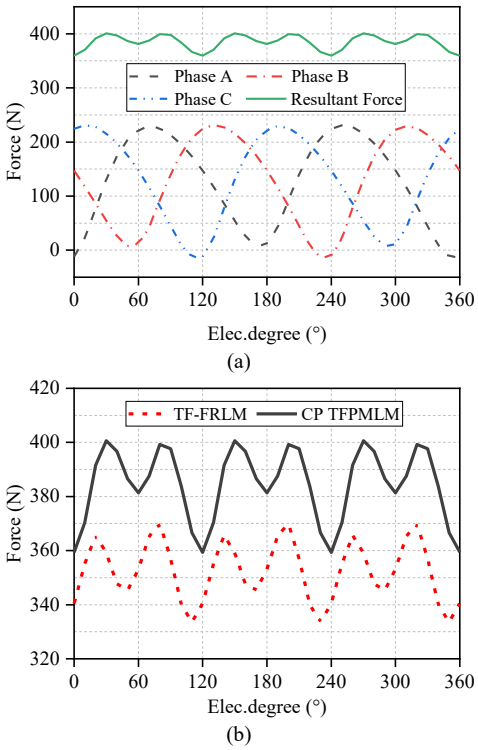

Fig. 10. Distribution of thrust force waveforms. (a) Thrust force of the CP TFPMLM. (b) Thrust force comparison at rated current.

be seen, the flux density varies in both direction with unequal amplitude. On the transversal direction, the flux density is a constant value under both PM pole and iron pole. The maximum value is obtained when the active part is in alignment with the secondary core. The maximum flux density under PM pole is about 0.71T and 0.45T for iron pole, while it is 0.4T and 0.11T, respectively, for the unalignment position. Along the longitudinal direction, the waveform of the air gap flux density distributed with a period of 2τ (τ = 7.5mm). The maximum flux density under PM pole is obtain when PM is in alignment with secondary cores, while the iron pole get its minimum value. The sunk wave under iron pole is caused by the inter-pole leakage of the magnets. When the iron pole is in alignment with secondary cores, the iron pole region obtains the maximum value. It can be seen that the flux density under iron poles is always in opposite direction with the PM poles.

B. No-load Flux Linkage and back EMF

Fig. 7 shows the waveforms of the single-phase CP TFPMLM. The amplitude of the CP TFPMLM is 86.9mWb. It has been promoted by about 25% compared to the TF-FRLM with the same magnet height and coil turns. The open-circuit EMF is shown in Fig. 8 at the velocity of 1m/s. The waveforms of the back EMF are not strictly sinusoidal but with high order harmonics. By applying Fourier transformation, the harmonic distribution is obtained. As can be seen, the third order harmonic is dominant in both machines. The fifth harmonic is much bigger in the CP TFPMLM. The fundamental amplitude of the CP TFPMLM is 34.29V, while it is 27.91V for the TF-FRLM. The fundamental amplitude is improved by 22.9% with consequent-pole configuration. The third harmonic amplitude of the CP TFPMLM is 4.79V, about 14% of the fundamental harmonic, while it is 8.4% for the TF-FRLM. However, the third harmonic can be eliminated by star connection of the windings.

C. Detent Force

The detent force is resulted from the interaction of magnets and magnetic material in the linear machine. The single-phase and three-phase detent force of the transverse flux linear

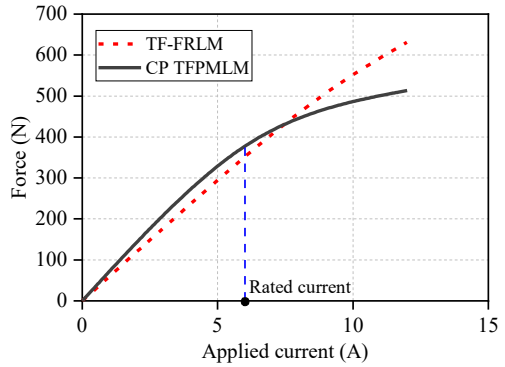

Fig. 11. Average value of three-phase thrust force versus applied current.

machine are indicated in Fig. 9. As observed, the three-phase detent force are drastically reduced when compared with the single-phase value. The maximum detent force of a single phase is about 125N for both kind machines. The peak force is unequal in an electrical period. The fluctuation is mainly caused by the end force effect. However, most of the harmonic orders has been cancelled out beside of the third and its integral times orders. The amplitude of the CP TFPMLM is 6N which is only half of the TF-FRLM's.

D. Thrust Force

Fig. 10 describes the thrust waveforms over an electrical period. The average thrust force of the CP TFPMLM is 384.4N, while it is 352.4N for the TF-FRLM. Hence, the thrust force of the proposed machine has improved by 9.1% at the same rated current even through the magnets has been reduced. Furthermore, a portion of negative thrust of a single-phase can be observed form Fig. 10 (a), which is caused by the detent force when the applied instantaneous current is relatively low. The CP TFPMLM has a force ripple of about 41.3N, which is a little higher than the TF-FRLM of 36.5N. The main reason is that the proposed machine is more easy to be saturated. Further, by increasing the applied current, the average thrust force changes as shown in Fig. 11. It can be found, when the applied current is under 7A, the average thrust force of the CP TFPMLM is higher than the TF-FRLM. Nevertheless, when the current keeps enlarged, the thrust force of the CP TFPMLM gains a little lower because of the saturation of the core. That is to say, the overload capacity of the CP TFPMLM is poor.

E. Demagnetization of Permanent Magnets

Fig. 12 shows the field distribution of permanent magnets under the maximum demagnetization current in different machines. As it can be seen, the operating point in the CP TFPMLM is much lower than that in the TF-FRLM. The lowest operating points occurs near the edges in the TF-FRLM. The average flux density in the magnets is about 0.6T. However, in the CP TFPMLM, the demagnetization area occurs mostly in the middle of the magnets. In this region, the flux density is about 0.3T. Hence, the magnets in the CP TFPMLM are more likely to be demagnetized at the same ampere-turns. Nevertheless, from another point of view, since the motor operating principle needs the permanent magnet to be demagnetized by the armature reaction magnetic field. The

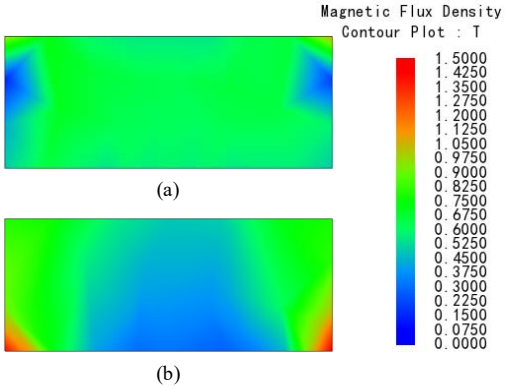

Fig. 12. Comparison of the magnetic field distribution of PMs under maximum instantaneous current. (a) TF-FRLM. (b) CP TFPMLM.

demagnetization effect is stronger in the CP TFPMLM, hence, the motor can also achieve a higher thrust force.

V. Conclusion

A consequent-pole permanent magnet linear machine has been proposed and investigated in this paper. By adopting of consequent-pole structure, the usage of permanent magnet material is saved and the overall manufacturing cost can be reduced. Nevertheless, the electromagnetic performance is barely impacted, or even has been improved. The flux linkage and back EMF are improved by 25% and 22.9%, respectively, while the detent force is reduced by near 50% when compared to its counterpart. The average thrust force was 9% higher than the TF-FRLM under the same rated current. But the proposed machine seems to be more sensitive to saturation influence and its overload capability is limited. Hence, the proposed machine is suitable for long stroke applications at continuous duty with the advantage of low cost.

References

[1] H. Weh and H. May, "Achievable force densities for permanent magnet excited machines in new configurations," in *Proc. Int. Conf. Electron.* Mach., Munchen, Germany, 1986, pp. 1107-1111.

[2] J. F. Pan, N. C. Cheung, and Y. Zou. "Design and analysis of a novel transverse-flux tubular linear machine with gear-shaped teeth structure," *IEEE Trans. Magn.*, vol. 48, no. 11, pp. 3339-3343, Nov. 2012.

[3] R. Watanabe, J. S. Shin, T. Koseki, and H. J. Kim. "Optimal design for high output power of transverse-flux-type cylindrical linear synchronous generator," *IEEE Trans. Magn.*, vol. 50, no. 11, pp. 1-4, Dec. 2014.

[4] P. Zheng, S. Zhu, B. Yu, L. Cheng and Y. Fan. "Analysis and Optimization of a Novel Tubular Staggered-Tooth Transverse-Flux PM Linear Machine." *IEEE Trans. Magn.*, vol. 51, no. 11, pp: 1-4, Nov. 2015.

[5] H. K. Do, H. J. Yeon and H. K. Moon, "A study on the design of transverse flux linear motor with high power density," in *ISIE 2001. 2001 IEEE International Symposium on Industrial Electronics Proceedings*, vol. 2, pp. 707-711, 2001.

[6] H. Polinder, B.C. Mecrow, A.G. Jack, P.G. Dickinson, and M.A. Mueller, "Conventional and TFPM linear generators for direct-drive wave energy conversion," *IEEE Trans. Energy Conver.,* vol. 20, no. 2, pp. 260-267, June 2005.

[7] C. Liu, G. Lei, B. Ma, Y. Wang, Y. Guo and J. Zhu, "Development of a new low-cost 3-d flux transverse flux FSPMM with soft magnetic composite cores and ferrite magnets," *IEEE Trans. Magn.,* vol. 53, no. 11, pp. 1-5, Nov. 2017.

[8] B. Kou, G. Yang, W. Zhou, and H. Zhang. "Bidirectional crosslinking

transverse flux flat type permanent magnet linear synchronous motor." *Proceedings of the CSEE*, vol. 32, no. 11, pp. 31-37, 2012.

[9] J. Shin, T. Koseki and H. Kim, "Proposal of double-sided transverse flux linear synchronous motor and a simplified design for maximum thrust in nonsaturation region," *IEEE Trans. Magn.,* vol. 49, no. 7, pp. 4104-4108, July 2013.

[10] J. Shin, R. Watanabe, T. Koseki, H. Kim and Y. Takada, "The design for cogging force reduction of a double-sided transverse flux permanent magnet linear synchronous motor," *IEEE Trans. Magn.,* vol. 50, no. 11, pp. 1-4, Nov. 2014.

[11] J. Shin, R. Watanabe, T. Koseki and H. Kim, "Practical design approach of a transverse flux linear synchronous motor for compact size, small mover weight, high efficiency, and low material cost," *IEEE Trans. Magn.,* vol. 51, no. 3, pp. 1-4, March 2015.

[12] J. Zou, M. Zhao, Q. Wang, J. Zou and G. Wu, "Development and analysis of tubular transverse flux machine with permanent-magnet excitation," *IEEE Trans. Ind. Electron.,* vol. 59, no. 5, pp. 2198-2207, May 2012.

[13] Q. Wang, Y. Xu, J. Hu, J. Zou and J. Zhang, "Enhancement of a thrust force of a tubular electromagnetic launcher with transverse flux configuration by leakage flux suppression," *IEEE Trans. Plasma Sci.,* vol. 41, no. 5, pp. 1150-1155, May 2013.

[14] D. H. Kang, Y. H. Chun and H. Weh, "Analysis and optimal design of transverse flux linear motor with PM excitation for railway traction," in *IEE Proceedings - Electric Power Applications,* vol. 150, no. 4, pp. 493-499, 8 July 2003.

[15] D. H. Kang and H. Weh, "Design of an integrated propulsion, guidance, and levitation system by magnetically excited transverse flux linear motor (TFM-LM)," *IEEE Trans. Energy Conver.,* vol. 19, no. 3, pp. 477-484, Sept. 2004.

[16] B. Kou, J. Luo, X. Yang, and L. Zhang, "Modeling and analysis of a novel transverse-flux flux-reversal linear motor for long-stroke application," *IEEE Trans. Ind. Electron.,* vol. 63, no. 10, pp. 6238-6248, Oct. 2016.

[17] M. Zhao, Y. Wei, H. Yang, *et al*, "Development and analysis of novel flux switching transverse flux permanent magnet linear machine," *IEEE Trans. Ind. Electron.,* vol. 66, no. 6, pp. 4923-4933, June 2019.

[18] S. Teymoori, A. Rahideh, H. Moayed-Jahromi, and M. Mardaneh, "2-D analytical magnetic field prediction for consequent-pole permanent magnet synchronous machines," *IEEE Trans. Magn.*, vol. 52, no. 6, pp. 1-14, June 2016.

[19] Z. Z. Wu and Z. Q. Zhu, "Comparative analysis of end effect in partitioned stator flux reversal machines having surface-mounted and consequent pole permanent magnets," *IEEE Trans. Magn.*, vol. 52, no. 7, July 2016.

[20] S. U. Chung, H. J. Lee, B. C. Woo, *et al*. "A feasibility study on a new doubly salient permanent magnet linear synchronous machine." *IEEE Trans. Magn.*, vol. 46, no. 6, pp. 1572-1575, June 2010.

[21] S. U. Chung, J. W. Kim, Y. D. Chun, *et al*. "Fractional slot concentrated winding PMSM with consequent pole rotor for a low-speed direct drive: reduction of rare earth permanent magnet." *IEEE Trans. Energy Conver*., vol. 30, no. 1, pp. 103-109, March 2015.

[22] D. Li, R. Qu, J. Li and W. Xu. "Design of consequent pole, toroidal winding, outer rotor vernier permanent magnet machines." *2014 IEEE Energy Conversion Congress and Exposition (ECCE),* Pittsburgh, PA, 2014, pp. 2342-2349.

Jun Luo (S'16) received the B.E. and M.E. degrees in electrical engineering in 2012 and 2014, respectively, from the Department Electrical Engineering, Harbin Institute of Technology, Harbin, China, where he is currently working toward the Ph.D. degree in electrical engineering from the Institute of Electromagnetic and Electronic Technology.

His research interests include novel permanent magnet linear motor design and optimization research.

Baoquan Kou (M'09) received the B.E. and D.E. degrees from Harbin Institute of Technology (HIT), China, in 1992 and 2004, respectively, and the M.E. degree from Chiba Institute of Technology, Japan, in 1995. He worked in the mobile station for the post doctors of HIT from 2005 to 2007. Since 2007, he has been a Professor in the School of Electrical Engineering and Automation, HIT.

His research interests include electric drive of electric vehicles, linear motors and linear electromagnetic drives, control of the power quality, and superconducting motors.

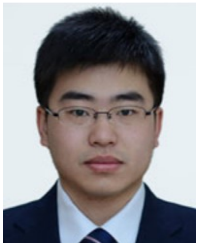

He Zhang (M'15) received the B.E., M.E., and Ph.D. degrees in electrical engineering from the Harbin Institute of Technology, Harbin, China, in 2008, 2010, and 2015, respectively. He is currently an Associate Professor with the Department of Electrical Engineering, Harbin Institute of Technology.

His research interests include the design and analysis of linear motor, planar motor, magnetic levitation gravity compensation, and eddy current damping.

Ronghai Qu (M'02–SM'05–F'18) received the B.E.E. and M.S.E.E. degrees in electrical engineering from Tsinghua University, Beijing, China, in 1993 and 1996, respectively, and the Ph.D. degree in electrical engineering from the University of Wisconsin-Madison, Madison, WI, USA, in 2002.

In 1998, he joined the Wisconsin Electric Machines and Power Electronics Consortiums as a Research Assistant. He became a Senior Electrical Engineer with Northland, a Scott Fetzer Company, New York, NY, USA, in 2002. Since 2003, he has been with the General Electric Global Research Center, Niskayuna, NY, USA, as a Senior Electrical Engineer with the Electrical Machines and Drives Laboratory. He has authored more than 260 published technical papers and is the holder of more than 135 patents/patent applications. Since 2010, he has been a Professor with Huazhong University of Science and Technology, Wuhan, China.